

Statistical Analysis of Small Ellerman Bomb Events

C.J. Nelson^{1,2} · J.G. Doyle¹ · R. Erdélyi² ·
Z. Huang¹ · M.S. Madjarska^{1,3} ·
M. Mathioudakis⁴ · S.J. Mumford² ·
K. Reardon^{4,5,6}

Received: 1 August 2012 / Accepted: 22 December 2012 / Published online: ●●●●●●●●

Abstract The properties of Ellerman bombs (EBs), small-scale brightenings in the $H\alpha$ line wings, have proved difficult to establish due to their size being close to the spatial resolution of even the most advanced telescopes. Here, we aim to infer the size and lifetime of EBs using high-resolution data of an emerging active region collected using the *Interferometric BIdimensional Spectrometer* (IBIS) and *Rapid Oscillations of the Solar Atmosphere* (ROSA) instruments as well as the *Helioseismic and Magnetic Imager* (HMI) onboard the *Solar Dynamics Observatory* (SDO). We develop an algorithm to track EBs through their evolution, finding that EBs can often be much smaller (around $0.3''$) and shorter lived (less than 1 minute) than previous estimates. A correlation between G-band magnetic bright points and EBs is also found. Combining SDO/HMI and G-band data gives a good proxy of the polarity for the vertical magnetic field. It is found that EBs often occur both over regions of opposite polarity flux and strong unipolar fields, possibly hinting at magnetic reconnection as a driver of these events. The energetics of EB events is found to follow a power-law distribution in the range of “nano-flare” (10^{22-25} ergs).

Keywords: Active Regions, Magnetic Fields- Magnetic fields, Photosphere- Sunspots, Penumbra

¹ Armagh Observatory, College Hill, Armagh, UK, BT61 9DG

² Solar Physics and Space Plasma Research Centre, University of Sheffield, Hicks Building, Hounsfield Road, Sheffield, UK, S3 7RH

³ UCL-Mullard Space Science Laboratory, Holmbury St Mary, Dorking, Surrey, UK, RH5 6NT

⁴ Astrophysics Research Centre, School of Mathematics and Physics, Queen’s University, Belfast, UK, BT7 1NN

⁵ INAF Osservatorio Astrofisico di Arcetri, I-50125 Firenze, Italy

⁶ National Solar Observatory / Sacramento Peak, P.O. Box 62, Sunspot, NM 88349, U. S. A.
email: c.j.nelson@sheffield.ac.uk

1. Introduction

Emerging active regions are some of the most diverse and abundant regions to study within the photosphere. Active regions possess a wide range of both large-scale (*e.g.* sunspots and pores) and small-scale (*e.g.* Ellerman bombs, also known as EBs) structures which, in a way that is yet to be fully understood, interact to form the complex overlying chromosphere. Here we study EBs, small-scale brightenings in the wings of the Balmer H α line profile, which occur in regions of high magnetic activity especially near opposite-polarity regions (see *e.g.* Georgoulis *et al.*, 2002, Pariat *et al.*, 2004).

Small-scale structures in the solar atmosphere have proved difficult to study due to their size being close to the spatial resolution of current observational instruments. EBs, possible magnetic reconnection events in the lower atmosphere due to emerging flux, are one such example. First reported by Ellerman (1917) and originally named “solar hydrogen bombs”, EBs have been reported to have a size of the order of one arcsecond (see *e.g.* Kurokawa *et al.*, 1982) and lifetime of around 10 – 15 minutes on average (see *e.g.* Vorpahl and Pope, 1972, Roy and Leparskas, 1973 and more recently Watanabe *et al.*, 2011). The energetics of EBs have been estimated by Georgoulis *et al.* (2002) and Fang *et al.* (2006), finding that each EB has a total lifetime energy of around 10^{27} ergs, a value typically associated with “micro-flares”. It has been widely acknowledged (*e.g.* Georgoulis *et al.*, 2002) that these estimates are upper bounds which will be revised occasionally by higher resolution, higher cadence data such as we present here.

The majority of investigations of EBs have been taken place the H α line wings. EB events, however, are also seen in other wavelengths such as the 1600 Å continuum and the Ca II wings (see, for example, Herlender and Berlicki, 2011). Recently, Qiu *et al.* (2000) suggested that over 50 % of EBs show a correlation to UV emissions in the 1600 Å continuum; a similar result was also found by Pariat *et al.* (2007), providing evidence that EBs are upper-photospheric, lower-chromospheric events.

Recently, a link has been suggested between EBs and G-band magnetic bright points (MBPs) (for a discussion of MBPs see Jess *et al.*, 2010a), which are ubiquitous in the solar photosphere. MBPs are the locations where the magnetic flux clumps together to form small magnetic concentrations with field strengths of the order of a kiloGauss (Stenflo, 1985). Their increased brightness is due to the reduced pressure and opacity within the flux tube allowing the observer to view a deeper, hotter region of the photosphere as well as heating of the plasma within the flux tube by material surrounding its walls. The increased temperature reduces the abundance of the CH molecule, thus making MBPs appear brighter in G-band imaging (Shelyag *et al.*, 2004). Jess *et al.* (2010b) has recently suggested that the interaction of neighbouring MBPs can lead to multiple EBs as a consequence of forced reconnection, thus hinting at a link between EBs and MBPs.

There have been a number of recent studies both on observations (Georgoulis *et al.*, 2002, Pariat *et al.*, 2007, Watanabe *et al.*, 2011) and modelling (Isobe, Tripathi, and Archontis, 2007, Archontis and Hood, 2009) of EBs. The main focus

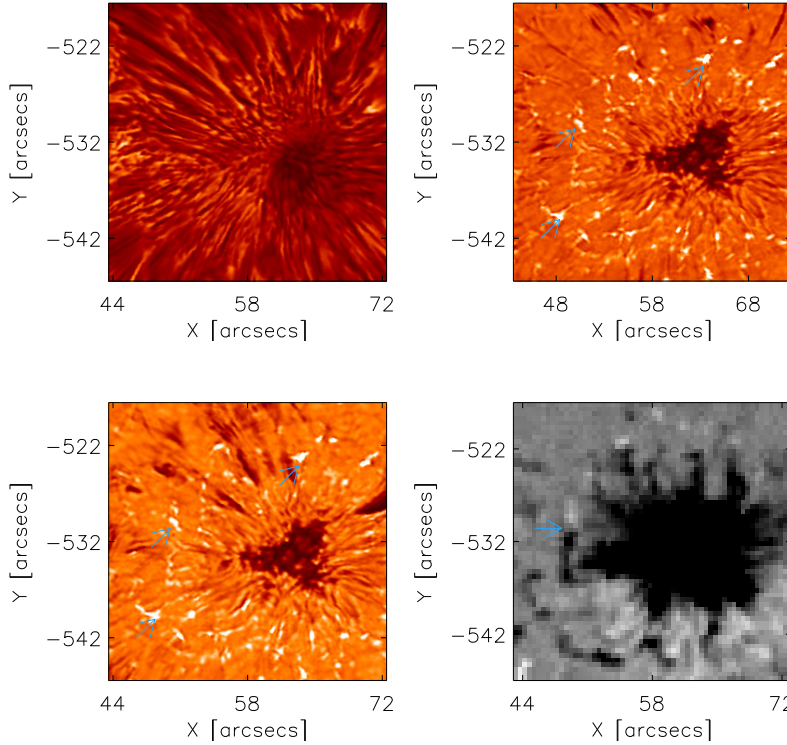


Figure 1. Images of Active Region NOAA 11126 (taken at 15:02:49) (a) at the $H\alpha$ line centre as well as (b)-(c) at $\pm 0.7 \text{ \AA}$, observed with DST/IBIS. Three EBs are shown with arrows. The same region is shown in (d), detected by the SDO/HMI instrument (using a threshold of ± 400 Gauss), which has been spatially and temporally aligned with (a-c).

of many of these studies has been to provide evidence for magnetic reconnection as the possible formation mechanism of EBs. A good cartoon was presented by Georgoulis *et al.* (2002), which depicts the possible magnetic topologies that could lead to magnetic reconnection in the lower-atmosphere either through emerging flux in bipolar regions or topologically complex unipolar fields. In this work, we find evidence that EBs are formed over regions of strong magnetic field, shown in both SDO/HMI data and the G-band continuum.

Magnetic reconnection is largely associated with high-energy events in the corona such as coronal mass ejections (CMEs) and large flares; however, in the past two decades, the applicability of the idea of magnetic reconnection to the lower-atmosphere has also been discussed. The process was described in Litvinenko (1999), who suggested that reconnection was likely to occur mainly around the temperature minimum region at $z \approx 600 \text{ km}$; this value does not appreciably disagree with the initial height of $z \approx 400 \text{ km}$ found by Harvey (1963). In Litvinenko, Chae, and Park (2007) it was suggested that lower-atmospheric magnetic reconnection is an important precursor that could lead to

larger events in the corona as well as mass supply into the chromosphere and corona through the ejection of cool photospheric plasma in the form of filaments.

EBs were originally thought to be precursors for flares; however, McMath, Mohler, and Dodson (1960) found this not to be the case through an analysis of a large array of data collected using a multitude of instruments in the preceding years. They did find, however, that EBs are mainly observed around the penumbra of active region sunspots; this has been discussed more recently by Pariat *et al.* (2004) who found that the majority of EBs occur in the trailing plage region. In this article we shall discuss the positioning of EBs identified in our dataset, finding formation to be common in both the unipolar penumbra and bipolar regions, in the surrounding active region close to the spot, suggesting both regions may have the required background conditions to form EBs. Madjarska, Doyle, and De Pontieu (2009) studied an $H\alpha$ surge, finding that the event was triggered by EBs forming in a similar spatial position. This is important as it could possibly suggest a coupling between the photospheric EB events and chromospheric $H\alpha$ surges.

We structure our study as follows: in Section 2 we discuss our observations and data reduction methods; Section 3 presents our results along with the definition we have used to calculate our statistics. Section 4 contains our conclusions and poses some questions that should be answered through further study.

2. Observations

In this article, we make use of high-resolution data collected by the *Interferometric Bidimensional Spectrometer* (IBIS) and *Rapid Oscillations of the Solar Atmosphere* (ROSA) instruments at the *Dunn Solar Telescope* (DST), *National Solar Observatory, Sacramento Peak, NM*, between 15:02 UT and 17:04 UT on 18 November 2010. We limit our analysis to the first 90 minutes of observations due to the deterioration of the seeing in the subsequent images (*i.e.* leaving 200 IBIS frames). IBIS data have a pixel size of $0.096''$ and, due to the excellent seeing, an approximate spatial resolution of $0.192''$. IBIS was set to produce a 15-point $H\alpha$ line scan (between $\pm 1.4 \text{ \AA}$ from the line centre in unequal steps) and 50 images in the line centre and both line wings at $\pm 0.7 \text{ \AA}$ before repeating this routine (*i.e.* a total of 165 images per cycle), sampling a total FOV of $96'' \times 96''$. G-band images from the ROSA instrument were collected during the same period with a cadence of 0.64 seconds (by combining 32 images, each with an integration time of 0.02 seconds), a pixel size of $0.059''$ and a spatial resolution of $0.118''$, covering a FOV of $58'' \times 58''$ (situated entirely within the IBIS FOV). We also use the *Helioseismic and Magnetic Imager* (HMI) onboard the *Solar Dynamics Observatory* (SDO) spacecraft, which has a pixel size of $0.5''$ a spatial resolution of $1''$ and a cadence of 45 seconds (whilst observing the whole disc). In Figure 1, we show context images with a field-of-view of $29'' \times 29''$ (to illustrate the complex region surrounding the sunspot) of the emerging active region NOAA 11126 at 31S latitude 00 longitude with co-aligned HMI and IBIS images. The DST tracked the leading spot, which evolved slowly through the time series. This spot was linked, by a coronal-loop arcade, to two small opposite-polarity spots situated in the trailing plage region.

Data analysis was conducted after two key steps: the speckle-imaging process and the alignment of the datasets. The speckle-imaging technique (Wöger, von der Lühse, and Reardon, 2008) was used for the IBIS line centre and wing data with each repetition of the IBIS routine contributing one final image with a cadence of 26.9 seconds. This process was applied to counteract the changes in seeing over the course of a single cycle by combining 50 short-burst images into a lower-cadence, higher-resolution image. For the ROSA G-band data, 32 images were used giving a final cadence of 0.64 seconds. Each $H\alpha$ speckle image was aligned to the previous image to eliminate jitter. Next, alignment of the datasets from separate instruments was carried out by co-aligning three specific reference points on each image and then rotating the images accordingly. Contour plots of the region as observed by DST/IBIS were then overlaid on SDO/HMI and DST/ROSA images with large features, such as the sunspot, used to validate the alignment.

Our $H\alpha$ observations have two main limitations that should be considered before future studies in this area are undertaken. Firstly, there is a cadence of 26.9 seconds which is large in comparison to the overall lifetime of network bright points (NBPs) as predicted by Watanabe *et al.* (2011) who note that the function $y \propto \exp(-x/C)$ fits the lifetimes and occurrence rates of NBPs well (where y is the number of NBPs for each lifetime, x). Therefore, our analysis is limited to events of lifetime longer than 54 seconds (or two consecutive frames) and could miss events that form and disappear within this time limit (brightenings that occur in one time frame are included in the histogram of lifetimes but are not included elsewhere). In Section 3.1, we discuss these shorter-lived events and how they link to EBs. Secondly, the spatial resolution of our data is potentially too large, at $0.192''$, to capture all EBs. EBs may form in much smaller areas than this. We do acknowledge that due to the speckling of the IBIS images, short-lived EBs may be missed; however, with the current observational techniques and the small scales of the events studied in this research, the compromise between high cadence and high spatial resolution is important.

3. Statistical Analysis

3.1. Identification of Ellerman Bombs

The definition of an Ellerman bomb (and its relationship to network bright points) varies widely within the literature on the topic. Here, we shall discuss, and justify, what we have found appropriate and used as the definition of an Ellerman bomb event and how this differs from those used by other authors. We suggest that, in essence, an Ellerman bomb is a brightening in the line wings of the $H\alpha$ optical line (an example is shown in Figure 2), which is also visible in the wings of other chromospheric lines such as Ca II as well as the 1600 Å continuum (Qiu *et al.*, 2000). In his original article studying the $H\alpha$ line profile, Ellerman (1917), suggested that the brightenings were “a very brilliant and very narrow band extending four or five Å on either side of the line, but not crossing it.” This definition still holds, suggesting that EBs are features of the upper photosphere

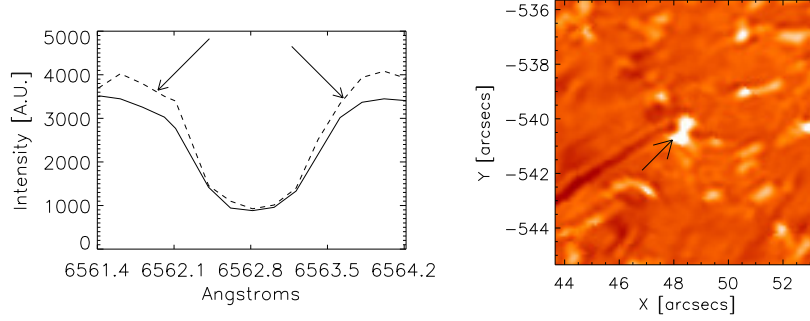


Figure 2. (a) $H\alpha$ line-profile showing an Ellerman bomb stretching out into the line wings. The solid line is from a quiet region and the dashed line is the profile for the EB indicated by the arrow in the blue wing image shown at 15:14:01 by (b). This EB is not taken from the same frame as Figure 1.

and lower chromosphere that are covered by the highly opaque network of fibrils and mottles that form the complex chromosphere, which it is possible to observe using the $H\alpha$ line centre.

The threshold at which an Ellerman bomb is no longer classified as a network bright point is also a point of interest. Recently, Watanabe *et al.* (2011) suggested that the difference between EBs and network bright points was both their brightness (EBs are more intense events) and their tendency to flare (both in intensity and size). This definition may, however, cause confusion, as smaller events that possess brightenings may not be observed flaring due to the “flare” being within the spatial resolution of the data. Here, we define an Ellerman bomb only in terms of brightening and set our threshold at 130 % of the average intensity of the image (this value is the upper limit of thresholds discussed in Georgoulis *et al.*, 2002). This value was chosen as it incorporated all major EB events selected by eye within this dataset as well as limiting the effect of the sunspot on the average FOV intensity.

Overall, we suggest and use the following as parameters for an automated method for the detection of EBs that can be implemented to follow their evolution through time:

- The region is over 130 % of the FOV average brightness in both the red and blue wings of the $H\alpha$ line-profile.
- It has an initial spatial overlap in the red and blue wings.
- Its area is greater than or equal to two pixels.
- If there is a spatial overlap in both the red and blue wings between frames then the EB is deemed to have lived into the next frame. After the initial frame, no overlap is required between the wings as small-scale events may separate within their lifetime.
- If there are multiple events with spatial overlap the one with the largest spatial correlation is taken; the others are neglected.

- Any EBs that occur in the first or last frame are removed from the sample so that only EBs with a complete lifetime are included.

Note that one of the main differences in the definition above from that by Watanabe *et al.* (2011) is that we do not set a lower time limit for the lifetimes of EBs (240 seconds is used in by Watanabe *et al.*, 2011). We discuss this change in Section 3.3. Any analysis on EB events should also take into account the original description by Ellerman (1917), in that EBs are not visible in the line centre. In this dataset there are no brightening events observed in the H α line centre during our time series, this was not included in the algorithm; however, this would potentially need to be revised for future studies.

EBs have been predicted to occur at a rate of 1.5 per minute in an $18'' \times 24''$ region by Zachariadis, Alissandrakis, and Banos (1987). Interpolating this to our FOV, we would expect around 30 EBs to occur per minute. Therefore in our 90-minute dataset we should expect to see 2690 EBs. Zachariadis, Alissandrakis, and Banos (1987) suggest that EBs can form, fade and recur in the same position meaning that 2690 could be extremely conservative. By classifying an event that rises above the 130 % threshold, fades and then rises above the threshold again as two separate events, we present 3570 EBs in this time range (133 % of the predicted value presented by Zachariadis, Alissandrakis, and Banos, 1987).

3.2. Spatial Occurrence of Ellerman Bombs

EBs form in highly magnetic regions, for example, in bipolar regions within emerging active regions or over complex unipolar topologies such as the penumbrae of sunspots (Georgoulis *et al.*, 2002). Figure 3 shows contours of the EBs from the same image at different brightness threshold values as well as an HMI image of the same region. The temporal alignment between the H α and HMI data is less than 10 seconds and we estimate that the spatial alignment is better than an arcsecond therefore within the spatial resolution of the HMI instrument.

The occurrence of EBs in emerging active regions such as NOAA 11126, which we study, has been used as evidence that they are magnetic reconnection events in the lower-atmosphere due to emerging flux (*e.g.* Georgoulis *et al.*, 2002). They have, previously, been predominantly observed between the leading spot and the following plage region; however, they have also been reported as occurring within complex penumbrae, where complex unipolar magnetic fields dominate (for flux emergence see Pariat *et al.*, 2004; for a good review of photospheric magnetic reconnection see Litvinenko, 1999). Both of these regions show strong and complex magnetic fields in photospheric magnetograms, therefore implying that magnetic fields are, in some way, responsible for the formation of EBs.

The FOV that we are observing is extremely complex in terms of magnetic field structuring. For example, we see from Figure 1(d) that there is a region of both positive and negative magnetic field indicated by the arrow to the left ($51''$, $-530''$) of the spot, which leads an intense brightening indicated by an arrow in Figures 1(b) and (c). Also, around the spot sits a large, penumbral structure as well as both small and large fibril structures (easily seen in Figure 1(c)).

We notice in Figure 3 that brighter EBs tend to form nearer to the strong magnetic fields within the penumbra of the leading spot. With a threshold of

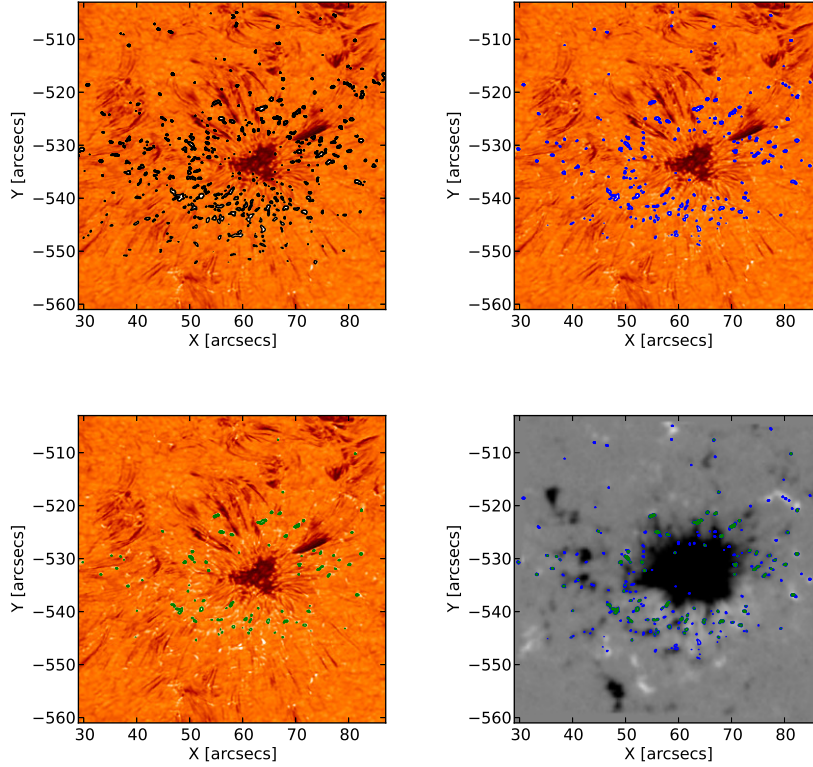


Figure 3. IBIS red wing images with contours of several brightness threshold values overplotted with: (a) 120 %, (b) 130 % and (c) 140 %, respectively. A temporally aligned HMI image (± 400 G) is included in (d) with 130 % and 140 % contours overplotted.

120 % we find a near-ubiquitous covering of EBs in the FOV, especially trailing the spot (to the left). As has been discussed previously, many of these events appear to be small, localised changes in the background intensity, which are selected by the algorithm due to the decreasing of the average FOV intensity caused by the sunspot. By increasing the intensity threshold to 130 %, many of the contours created at 120 % disappear and leave what, by eye, appears to be all major EB events. A threshold of 140 % focuses the brightenings around the spot at the regions of highest magnetism (Figure 3(c)); however, several examples of large, flaring brightenings are not selected with this threshold, implying that it may be too high.

The spatial correlation between EBs and strong vertical magnetic field, as shown in Figure 3(d), is another hint that EBs are in fact magnetic events whose intensity is dominated by the strength of the magnetic field. By contouring EBs identified with thresholds of 130 % and 140 % on a temporally aligned SDO/HMI magnetogram, it is easy to see the correlation between $H\alpha$ brightenings and strong magnetic fields. At approximately $(55'', -543'')$, one can pick out a line of negative polarity magnetic field that is mirrored exactly by EBs. An example

at a region of positive polarity can be seen at $(80'', -519'')$. The cadence and, more importantly, the spatial resolution of the HMI images are, however, too low to pick out fine-scale structuring within the magnetic field meaning nothing more than a correlation between EBs and strong, vertical photospheric magnetic fields is supported by this analysis. Higher-resolution magnetograms are required to fully analyse whether EBs are associated with separatrix of magnetic structures as suggested by Georgoulis *et al.* (2002).

3.3. Lifetime of Ellerman Bombs

Previous studies of EBs have been limited by relatively long-cadence observations (the Flare Genesis Experiment used by Georgoulis *et al.*, 2002, and Pariat *et al.*, 2004, for example, had a cadence of ≈ 3.5 minutes) except for a small number of key studies (*e.g.* Watanabe *et al.*, 2011), which could miss the formation of EBs. Here, we present an analysis of EB lifetimes using high-resolution, relatively high-cadence observations. The speckle reconstruction technique we applied has improved the spatial resolution of these data, meaning that even brightenings of around $0.14''$ are observable with a temporal cadence of 26.9 seconds. The resolution of our data in both spatial and temporal coordinates allows us to detect EBs both occurring and, more importantly, recurring (see *e.g.* Georgoulis *et al.*, 2002), which influences previous lifetime estimates.

In Figure 4(a), we show a histogram of the lifetimes of EBs for our dataset. We find that the function $y \propto \exp(-x/C)$ (where y and x are the total number and lifetime of EBs respectively and $C = 2.7 \pm 0.16$) proposed by Watanabe *et al.* (2011) fits our histogram for lifetimes less than 20 minutes, implying the possibility that EBs could be formed and disappear on timescales shorter than the temporal resolution presented here. Even higher cadence is required to fully answer this question. Although the fit of this curve appears to have a long tail, it should be noted that only seven events do not match the the exponential function, meaning that 5402 events do fit this curve.

We suggest that EBs can be much shorter-lived than previous estimates and that in fact they can be shorter than our cadence. By considering only the 3570 EBs with lifetimes over one frame, we find an average lifetime of approximately three minutes which is considerably less than previous estimates of five to ten minutes. We find that for 5409 EBs (including those EB events only observed in one frame), the average lifetime drops to approximately two minutes suggesting that this research may only present an upper limit on lifetime. To check the reliability of the algorithm, large events (over the $0.8''$ spatial-resolution presented by Georgoulis *et al.*, 2002) are also analysed (histogram plotted in blue in Figure 4(a)) giving an average lifetime for these events of approximately eight minutes. A continued trend, as seen in Figure 4(a), coupled with Figure 4(b) could suggest that small magnetic reconnection events are extremely common in emerging active regions especially at the outer penumbra (see Figure 3) as well as the surrounding quiet Sun. We suggest that a higher cadence dataset would find even shorter-lived EB events than presented here as well as better accounting for their recurrence.

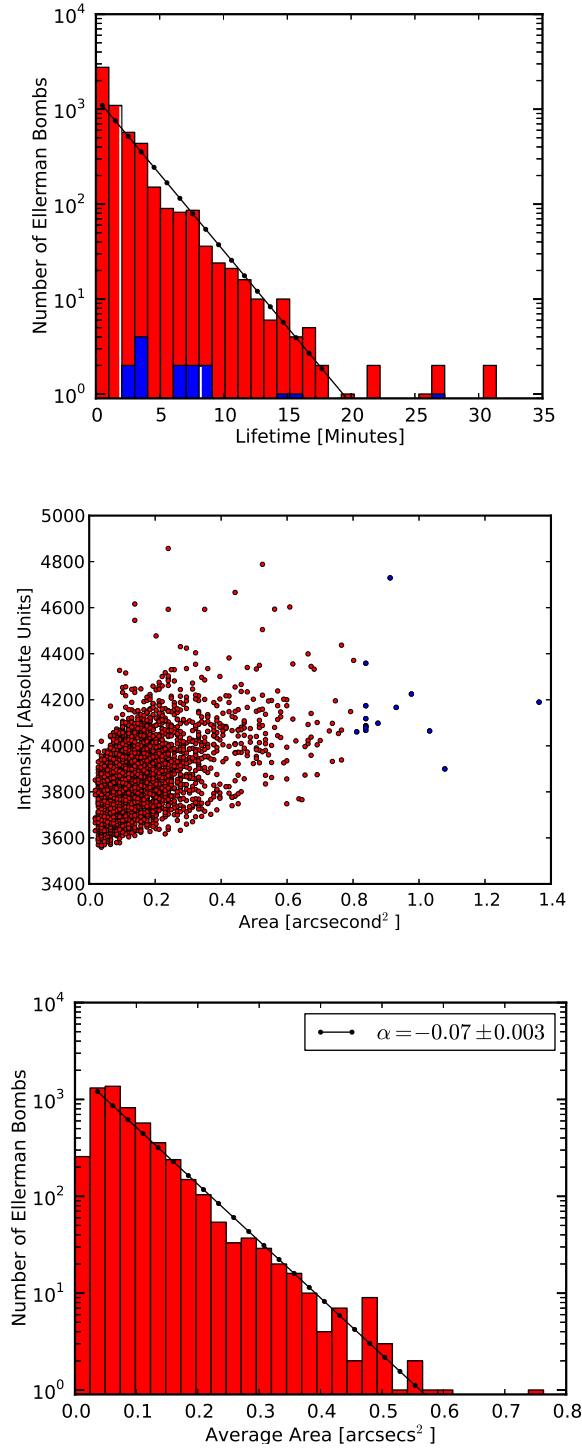


Figure 4. (a) Ellerman bomb lifetime frequency plot. EBs with area larger than $0.8'' \times 0.8''$ (circular diameter of approximately $0.45''$) are shown using blue to compare estimates with previous researches. (b) Intensity by area plot. Again, blue indicates larger events and red shows smaller events. (c) A histogram of area against $\log(\text{frequency})$.

3.4. Area of Ellerman bombs

EBs have been described as slightly elliptical brightenings with size of the order $1''$ (for example Zachariadis, Alissandrakis, and Banos, 1987, Georgoulis *et al.*, 2002) such as in Figure 2. Our definition of EBs gives a large number of extremely small, less bright examples as shown in Figure 3. An intuitive explanation for this is that the spatial and temporal resolution that are used here, for example, are one-fifth and one-seventh of the Flare Genesis Experiment resolutions, respectively. We find that the majority of EBs in this study have diameters of below $0.5''$ and find only a small number (15 over $0.8'' \times 0.8''$ at some point in their lifetime) with areas comparable to previous studies.

The evolution of EBs over time is dominated by dynamic changes that were interpreted by Watanabe *et al.* (2011) as flaring. This flaring can consist of the rapid extension of thin “arms” away from the main structure or of a more general area expansion. We suggest that EBs that have an area of the order of our spatial resolution may still flare but, if this is at the same ratio as larger flaring EBs, this will not be picked up by these observations. By analysing large events we do find some evidence of flaring within EBs through their lifetime; however, not all EBs, as identified in this study, can be seen to change visibly in either area or shape. We suggest that flaring may be a special case and not a defining feature of EB formation.

Here, we find a plethora of small EB events (which are easily picked out in Figure 3 and are shown in Figures 4(b) and (c)) as well as many larger, more well-defined events. A positive correlation between the area and brightness of EBs is observed, implying the energy released from larger events is more powerful than the energy of smaller events. It should be noted that the small events have been missed due to both the spatial and temporal resolution of studies by *e.g.* Georgoulis *et al.* (2002) or Pariat *et al.* (2004); however, with the spatial resolution in the current data, and the availability of the aligned SDO/HMI data (Figure 3), we are able to observe that many of these events are spatially linked to the approximate vertical magnetic field. This implies that many of the smaller events neglected in Watanabe *et al.* (2011) may be EB events on a smaller scale. In Section 3.6, we shall use high-resolution G-band data as a proxy for the magnetic field to discuss the formation of both the larger and smaller events.

3.5. Movement and recurrence of Ellerman bombs

The formation of Ellerman bomb events due to the movement of G-band magnetic bright points has been discussed by Jess *et al.* (2010b), who found that MBPs that migrate along the intergranular lanes can form the foot-points of $H\alpha$ micro-flare events. They reported a constant velocity of 1 km s^{-1} and 1.8 km s^{-1} for two G-band MBPs, which is matched well to the estimated MBP horizontal velocity stated by Utz *et al.* (2010). Keys *et al.* (2011) extended this work, discussing the differences between isolated MBPs and merging MBPs. Interestingly, their results showed agreement with those found by Utz *et al.* (2010) in that isolated MBPs have an average velocity of around 1 km s^{-1} ;

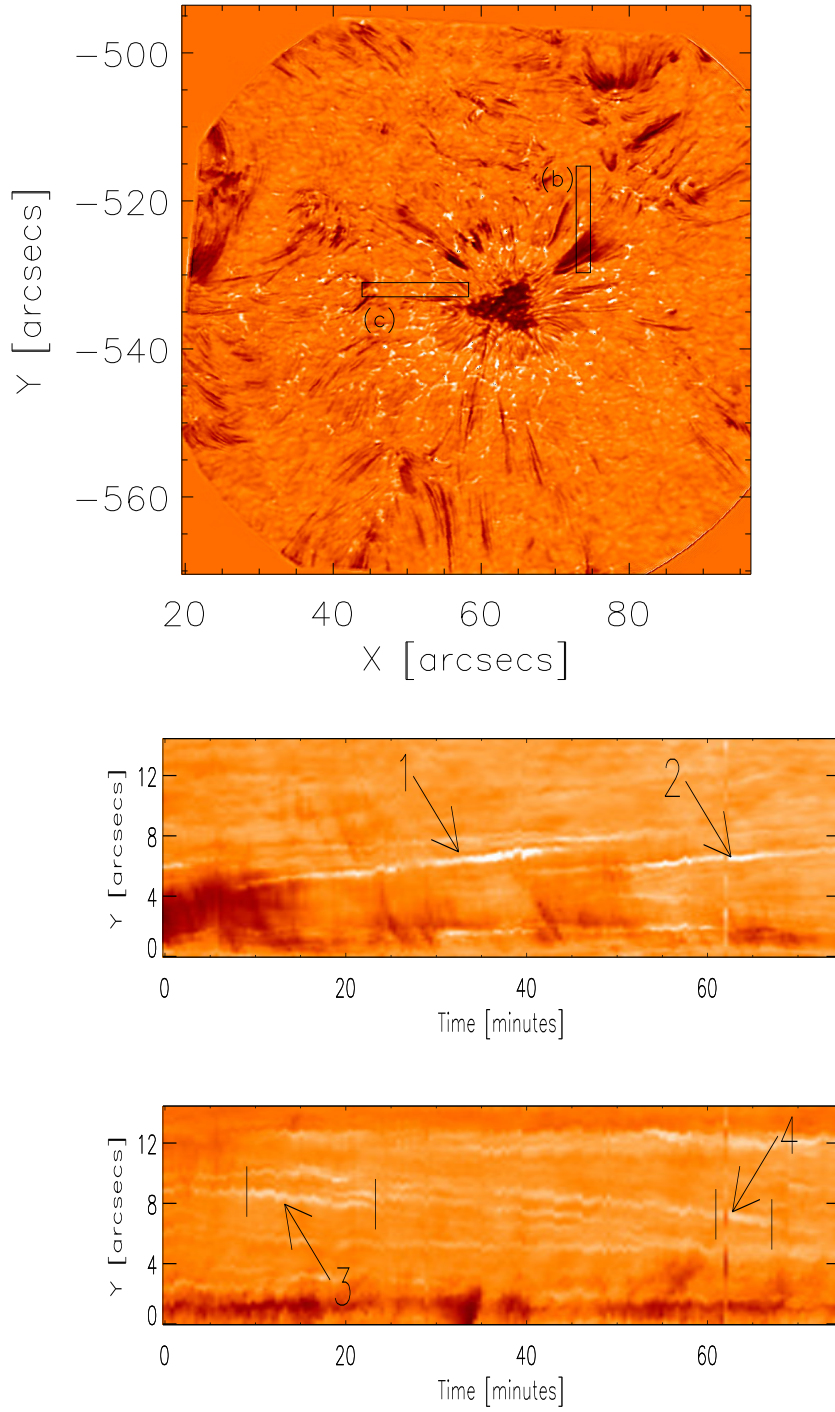


Figure 5. (a) Full FOV red wing image at time = 0. (b) Space-time plot calculated by averaging the x -axis intensities over slit (b) (20 pixels wide) in the full FOV image. Brightenings 1 and 2 occur from a similar spatial position and then migrate away from the spot. (c) Space-time plot corresponding to slit (c) from the full FOV image.

however, they found that merging MBPs appeared to have significantly larger velocities. Should MBPs and EBs possibly be linked, as discussed previously, then one should expect motions to also be seen in EB events. Georgoulis *et al.* (2002) and Watanabe *et al.* (2011) both studied EB movements within the $H\alpha$ line wings, finding horizontal motions of the order of 0.4 to 0.8 km s⁻¹. Here, we discuss the velocities of typical EB motions associated with recurring events (presented in Figure 5).

Figure 5(b) shows the horizontal motions of two EBs that occur from a similar spatial position and then migrate away from the sunspot with characteristic speeds around 1 km s⁻¹. The brightenings form and become more pronounced over time becoming defined as EBs (over 130 % of the average image intensity) before fading away. We found that around half an hour after the initial brightening there is a second occurrence from the same position. Each trail is only characterised as an Ellerman bomb for a short amount of time due to rapid brightening and fading. We mark the first brightening with “1” and the second with “2”. The recurrence of an EB from a similar spatial position could be interpreted as a continued emergence of flux leading to multiple reconnection and, therefore, EB events.

The lower panel, Figure 5(c), shows the second definition of recurrence that is prevalent in these observations. We find many examples of extreme brightenings, classified as EBs, fading before becoming brighter again. Bars are situated around the EBs indicated by arrows 3 and 4 to show the extent of the lifetime of each event. One should note, however, that this is an x-t plot and, therefore, does not accurately convey relative brightness (*e.g.* if a full 20 pixels are around 110 % of the background brightness, this may appear similar to a ten pixel 130 % brightness). To make this plot, we analysed a movie of the same period over time and noted that the EBs that are indicated by the bars appear to be connected. We find that many EBs tend to fade before regaining brightness at a later time, perhaps due to a recurrence of a triggering event such as magnetic reconnection. Over the course of its lifetime this EB/sustained brightening has a velocity of approximately 0.4 km s⁻¹, which is consistent with velocities found by Georgoulis *et al.* (2002) and Watanabe *et al.* (2011).

3.6. Correlation Between G-band Magnetic Bright Points and EBs

Current theories of EBs suggest that they are likely to be formed through magnetic reconnection in the lower solar atmosphere. In this Section we use G-band/ROSA data as a proxy for the magnetic field (Berger and Title, 2001; De Wijn *et al.*, 2009) in the photosphere to further discuss this idea. MBPs observed in the G-band wavelength are created by the build-up of magnetic flux within inter-granular lanes deposited by their associated down-drafts, thereby leading to significant brightenings. A connection between G-band MBPs and EBs is discussed by Jess *et al.* (2010b) who found that brightening events in the $H\alpha$ line wings can be spatially correlated to MBPs in the G-band. We expand on their work here by discussing examples of both large and small EBs and their relation to MBPs.

We define a large EB to have an area of approximately 0.8'' \times 0.8'', the approximate average EB size in *e.g.* Georgoulis *et al.* (2002) and Watanabe *et al.*

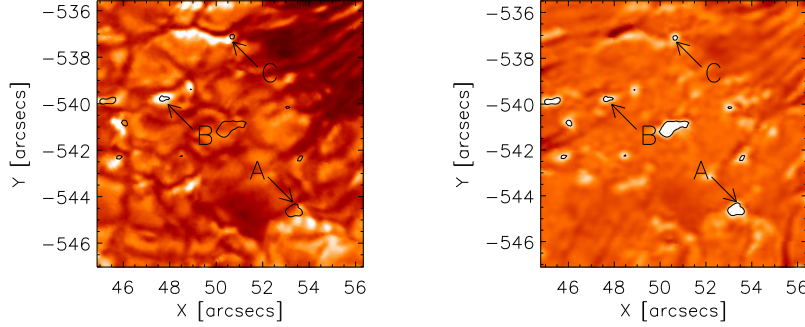


Figure 6. (a) G-band image with EBs contoured over it in white. Correlation between many brightenings is evident; three characteristic examples are shown with arrows. (b) Temporally aligned $H\alpha$ blue wing image with the arrows pointing to the EBs shown in (a).

(2011). By co-aligning the $H\alpha$ line-wing and G-band datasets, we find that there is a correlation between many EB brightenings and MBPs. EB *A* in Figure 6, for example, is a large EB situated over an inter-granular lane and linked to photospheric bright points in the G-band image. As has been shown by *e.g.* Jess *et al.* (2010b), large EBs can possibly be caused by interactions between two photospheric MBPs within inter-granular lanes. Note, as this sunspot is south of the disk-centre, MBPs will not appear within the inter-granular lanes; rather the southern walls of the event will appear below the dark lanes as with events *A*, *B* and *C*.

Examples exist within this FOV that do not correlate to brightenings within the G-band image (most noticeably at $(51'', -541'')$). We suggest that this is due to MBPs being a possible proxy for strong vertical magnetic field within G-band data and EBs potentially being the product of magnetic reconnection, which does not necessarily occur only at sites of vertical field. This implies, therefore, that G-band MBPs can lead to the formation of EBs, although, not in every case, and that EBs can form without interaction between MBPs. This supports models suggested by, for example, Georgoulis *et al.* (2002), whereby multiple magnetic topologies can lead to EB formation.

We now discuss smaller EB events such as *B* and *C* from Figure 6. The co-aligned data allow us to observe that these smaller EB events can also be linked to MBPs within the G-band dataset. EB *C* does not increase in size from this image throughout its short lifetime. These two typical examples show a similar spatial relationship between MBPs within intergranular lanes and small EB events as that possessed by larger EB events. It has been reported that two MBPs interacting can create EB brightenings in the $H\alpha$ line wings; however, for events *B* and *C*, we see no evidence of fragmented MBPs (*i.e.* only one MBP is observable). Whether fragmenting occurs on scales smaller than the spatial-resolution presented here will be answered by higher-resolution data.

We suggest that the potential link between small EBs and MBPs supports the assertion that the smaller events, which have been neglected in other studies,

are indeed EB events. De Wijn *et al.* (2009) proposed that magnetic structuring within the photosphere should happen on a spatial scale well below the diffraction limit of current telescopes; this has been supported by numerical simulations run by Crockett *et al.* (2010) who found the mode MBP size to be around 45 000 km² (or a circular diameter of approximately 0.32'') and an equal number of events with sizes 10 000 km² and 100 000 km² (circular diameters of 0.16'' and 0.49'', respectively). Therefore, if there is a connection between magnetic structuring and EBs as widely anticipated (Georgoulis *et al.*, 2002; Pariat *et al.*, 2004; Jess *et al.*, 2010b; Watanabe *et al.*, 2011), then high-resolution data, collected during periods of excellent atmospheric seeing, as presented here, should find EBs to be, on average, extremely small which is supported by our results from Figures 4(b) and (c). Both the cadence and resolution of modern telescopes need to be improved to conclusively establish whether these smaller events have the same properties as larger EBs in terms of morphology; however, we have shown that these small EB events do appear to have the same driver from the lower photosphere and that they are, therefore, worthy of further study.

3.7. Energetics

We have found that EBs are numerous and intense in the wings of the H α line profile around the active region sunspot that we have studied. Georgoulis *et al.* (2002) estimated the energies of each EB at its peak, P_{rad} , and in total, E_{rad} ; we shall conduct a similar analysis on the EBs identified by the algorithm used this work as follows:

$$P_{\text{rad}} \approx \epsilon_{\text{rad}} f V_{\text{EB};\text{max}} \quad \text{and} \quad E_{\text{rad}} \approx \frac{P_{\text{rad}} D}{2} \quad (1)$$

where ϵ_{rad} is the net radiative loss rate estimated by:

$$\epsilon_{\text{rad}} \approx a(T) n^2 \chi g(T), \quad (2)$$

f is the radiative filling factor (assumed as being unity), $V_{\text{EB};\text{max}}$ is the maximum volume of the EB and D is the lifetime of each EB. Defining $a(T)$ as the radiative reduction coefficient, n as the total numerical density of electrons and neutral hydrogen, χ as the ionization degree and $g(T)$ as a semi-empirical function of the temperature from Nagai (1980) and assuming $T \approx 10^4$ K and $n \approx 10^{12}$ cm⁻³, Georgoulis *et al.* (2002) found $\epsilon_{\text{rad}} \approx 0.89$ erg cm⁻³ s⁻¹. Letting the height of an average EB be 10² kilometres, we are able to produce estimates for the maximum and total energies of each of our EBs (Figure 7).

We find that the energetics of the EBs studied in this article are around three to four orders of magnitude smaller than those stated in Georgoulis *et al.* (2002). A log-log plot of the number of EBs with respect to energy is plotted in Figures 7(a) and (b) appearing to show a power-law function ($dN(x)/dx \propto x^{-\alpha}$). Fits are plotted for both the total and maximum energy release graphs finding power law indices of $\alpha_{\text{total}} = -1.00 \pm 0.04$ and $\alpha_{\text{max}} = -2.14 \pm 0.08$ respectively. Interestingly, the total energy release histogram shows energies in the region $[2 \times 10^{22}, 4 \times 10^{25}]$ ergs, which has been suggested as the possible energies of

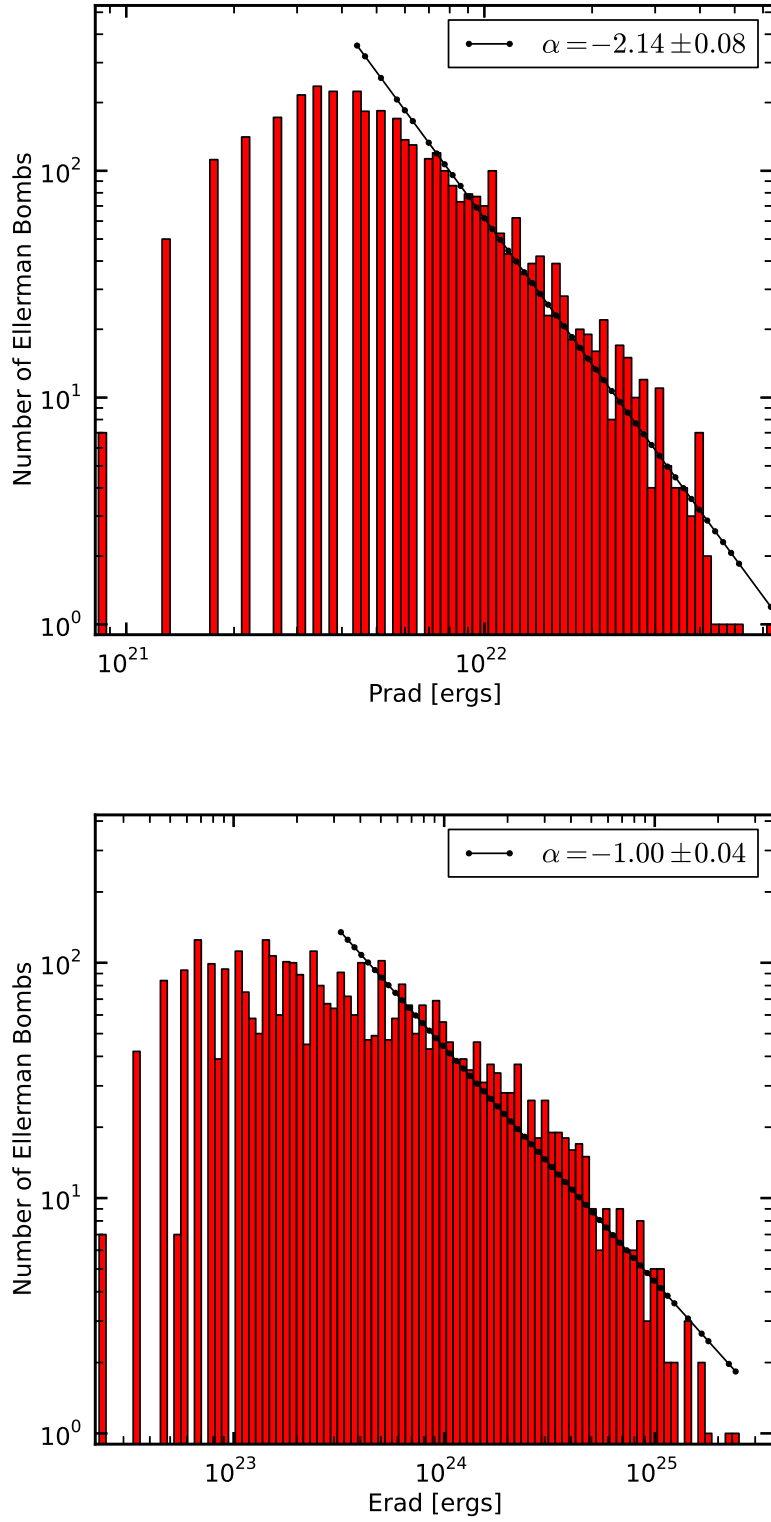


Figure 7. (a) The maximum energy of each EB. (b) The total energy release for each EB taking into account the estimated lifetime of each EB from our study.

“nano-flares” by Parnell and Jupp (2000). We note that the power law that fits the total energy release does not imply that EBs are a major contributor to coronal heating; however, we suggest that this relation could be changed by higher temporal and spatial resolution data (*i.e.* by only including larger, longer-lived events where limitations in the observational resolutions are less evident, the power law changes so that $\alpha_{\text{total}} > 2$ and, therefore, EBs have the required energy to sustain the corona).

We firmly remind the reader that these values are based on a large number of, possibly erroneous, assumptions such as the height over which EBs form, the temperature and total numerical densities stated here. For example, the temperature given in this work, $T \approx 10^4$ K, is, perhaps, a factor of two larger than average photospheric temperatures. The individual brightness of each event is also not included in this method, therefore not differentiating between extremely bright, high-energy events, and less bright, low-energy events. Overall, we suggest that the estimates of EB energies presented in this article should be a topic of consideration for future studies. The

4. Conclusions

The strong magnetic fields in the solar atmosphere are believed to be one of the key components that link the photosphere and the lower atmosphere to the corona and upper atmosphere. Here, we have discussed EBs, one possible manifestation of magnetic reconnection in the lower-atmosphere, concentrating on their morphology and statistical properties.

We find that the inclusion of “flaring” in the definition of EBs leads to the omission of many small-scale (less than $0.8''$) events that have the same signatures as larger, more widely studied EB brightenings in the $H\alpha$ line wings. Analysing the lifetimes and area of over 3500 EB events, we find an average lifetime of 2 – 3 minutes, much less than previous estimates, which have ranged from 5 – 15 minutes (*e.g.* Georgoulis *et al.*, 2002; Pariat *et al.*, 2004; Watanabe *et al.*, 2011) and also a decreased average area. To test the algorithm, events over the spatial resolution of previous researches were also analysed, allowing us to retrieve a lifetime estimate comparable to previous studies that did not benefit from the high-resolution, high-cadence data that are used here.

Additionally, we find that the underlying G-band photospheric data show corresponding brightenings to intense $H\alpha$ brightenings even at a scale around $0.2''$. These smaller events also show diminished energies from previous studies with our dataset yielding energies of between $[2 \times 10^{22}, 4 \times 10^{25}]$ ergs for the 3570 EBs studied. These energies also hint at a power law shape, which should be expanded upon by further studies. This agrees well with the theory presented by De Wijn *et al.* (2009), who suggested that magnetic reconnection and structuring can happen well below current observational resolution and cadence. The continued advancement of observational instruments should lead to more detailed studies of these small events to discuss their morphology in comparison to larger events.

Overall, we find the EBs are short-lived, small-scale events that are common in the $H\alpha$ line wings around active region sunspots. They form over bipolar

regions with complex mixing magnetic polarities (as inferred from the SDO/HMI instrument) as well as within and around the edges of strong penumbrae (either through unipolar magnetic field interactions within the penumbra or bipolar fields in the surrounding region). If evidence of magnetic reconnection leading to EBs in the lower-atmosphere is found, it is possible that they could prove an excellent driver of jets into the transition region and even, possibly, into the corona.

Acknowledgements Research at the Armagh Observatory is grant-aided by the N. Ireland Dept. of Culture, Arts and Leisure. We thank the National Solar Observatory / Sacramento Peak for their hospitality and in particular Doug Gilliam for his excellent help during the observations. We thank the UK Science and Technology Facilities Council for the studentships (CJN and SJM), PATT and support, plus support from grant ST/J001082/1. RE is thankful to the NSF, Hungary (OTKA, Ref. No. K83133) and acknowledges M. K  ray for patient encouragement. We thank Friedrich W  ger for his Image Reconstruction code and S. B. Nicholson for the connected objects algorithm adapted for this study. The research leading to these results has received funding from the European Commission’s Seventh Framework Programme (FP7/2007-2013) under the grant agreement eHeroes (project no. 284461, <http://www.eheroes.eu>). MM would like to thank the Air Force Office of Scientific Research, Air Force Material Command, USAF for sponsorship under grant number FA8655-09-13085. HMI data courtesy SDO (NASA) and the HMI consortium.

References

- Archontis, V., Hood, A.W.: 2009, Formation of Ellerman bombs due to 3D flux emergence. *Astron. Astrophys.* **508**, 1469–1483. doi:10.1051/0004-6361/200912455.
- Berger, T.E., Title, A.M.: 2001, On the Relation of G-Band Bright Points to the Photospheric Magnetic Field. *Astrophys. J.* **553**, 449–469. doi:10.1086/320663.
- Crockett, P.J., Mathioudakis, M., Jess, D.B., Shelyag, S., Keenan, F.P., Christian, D.J.: 2010, The Area Distribution of Solar Magnetic Bright Points. *Astrophys. J. Lett.* **722**, L188–L193. doi:10.1088/2041-8205/722/2/L188.
- De Wijn, A.G., Stenflo, J.O., Solanki, S.K., Tsuneta, S.: 2009, Small-Scale Solar Magnetic Fields. *Space Sci. Rev.* **144**, 275–315. doi:10.1007/s11214-008-9473-6.
- Ellerman, F.: 1917, Solar Hydrogen “bombs”. *Astrophys. J.* **46**, 298. doi:10.1086/142366.
- Fang, C., Tang, Y.H., Xu, Z., Ding, M.D., Chen, P.F.: 2006, Spectral Analysis of Ellerman Bombs. *Astrophys. J.* **643**, 1325–1336. doi:10.1086/501342.
- Georgoulis, M.K., Rust, D.M., Bernasconi, P.N., Schmieder, B.: 2002, Statistics, Morphology, and Energetics of Ellerman Bombs. *Astrophys. J.* **575**, 506–528. doi:10.1086/341195.
- Harvey, J.W.: 1963, Height of an Ellerman “bomb”. *The Observatory* **83**, 37–38.
- Herlender, M., Berlicki, A.: 2011, Multi-wavelength analysis of Ellerman Bomb Light Curves. *Central European Astrophysical Bulletin* **35**, 181–186.
- Isobe, H., Tripathi, D., Archontis, V.: 2007, Ellerman Bombs and Jets Associated with Resistive Flux Emergence. *Astrophys. J. Lett.* **657**, L53–L56. doi:10.1086/512969.
- Jess, D.B., Mathioudakis, M., Christian, D.J., Crockett, P.J., Keenan, F.P.: 2010a, A Study of Magnetic Bright Points in the Na I D₁ Line. *Astrophys. J. Lett.* **719**, L134–L139. doi:10.1088/2041-8205/719/2/L134.
- Jess, D.B., Mathioudakis, M., Browning, P.K., Crockett, P.J., Keenan, F.P.: 2010b, Microflare Activity Driven by Forced Magnetic Reconnection. *Astrophys. J. Lett.* **712**, L111–L115. doi:10.1088/2041-8205/712/1/L111.

- Keys, P.H., Mathioudakis, M., Jess, D.B., Shelyag, S., Crockett, P.J., Christian, D.J., Keenan, F.P.: 2011, The Velocity Distribution of Solar Photospheric Magnetic Bright Points. *Astrophys. J. Lett.* **740**, L40. doi:10.1088/2041-8205/740/2/L40.
- Kurokawa, H., Kawaguchi, I., Funakoshi, Y., Nakai, Y.: 1982, Morphological and evolutionary features of Ellerman bombs. *Solar Phys.* **79**, 77–84. doi:10.1007/BF00146974.
- Litvinenko, Y.E.: 1999, Photospheric Magnetic Reconnection and Canceling Magnetic Features on the Sun. *Astrophys. J.* **515**, 435–440. doi:10.1086/307001.
- Litvinenko, Y.E., Chae, J., Park, S.-Y.: 2007, Flux Pile-up Magnetic Reconnection in the Solar Photosphere. *Astrophys. J.* **662**, 1302–1308. doi:10.1086/518115.
- Madjarska, M.S., Doyle, J.G., De Pontieu, B.: 2009, Explosive Events Associated with a Surge. *Astrophys. J.* **701**, 253–259. doi:10.1088/0004-637X/701/1/253.
- McMath, R.R., Mohler, O.C., Dodson, H.W.: 1960, Solar Features Associated with Ellerman's "Solar Hydrogen Bombs". *Proceedings of the National Academy of Science* **46**, 165–169. doi:10.1073/pnas.46.2.165.
- Nagai, F.: 1980, A model of hot loops associated with solar flares. I - Gasdynamics in the loops. *Solar Phys.* **68**, 351–379. doi:10.1007/BF00156874.
- Pariat, E., Aulanier, G., Schmieder, B., Georgoulis, M.K., Rust, D.M., Bernasconi, P.N.: 2004, Resistive Emergence of Undulatory Flux Tubes. *Astrophys. J.* **614**, 1099–1112. doi:10.1086/423891.
- Pariat, E., Schmieder, B., Berlicki, A., Deng, Y., Mein, N., López Ariste, A., Wang, S.: 2007, Spectrophotometric analysis of Ellerman bombs in the Ca II, H α , and UV range. *Astron. Astrophys.* **473**, 279–289. doi:10.1051/0004-6361:20067011.
- Parnell, C.E., Jupp, P.E.: 2000, Statistical Analysis of the Energy Distribution of Nanoflares in the Quiet Sun. *Astrophys. J.* **529**, 554–569. doi:10.1086/308271.
- Qiu, J., Ding, M.D., Wang, H., Denker, C., Goode, P.R.: 2000, Ultraviolet and H α Emission in Ellerman Bombs. *Astrophys. J. Lett.* **544**, L157–L161. doi:10.1086/317310.
- Roy, J.-R., Leparskas, H.: 1973, Some Statistical Properties of Ellerman Bombs. *Solar Phys.* **30**, 449–457. doi:10.1007/BF00152675.
- Shelyag, S., Schüssler, M., Solanki, S.K., Berdyugina, S.V., Vögler, A.: 2004, G-band spectral synthesis and diagnostics of simulated solar magneto-convection. *Astron. Astrophys.* **427**, 335–343. doi:10.1051/0004-6361:20040471.
- Stenflo, J.O.: 1985, Measurements of magnetic fields and the analysis of Stokes profiles. *Solar Phys.* **100**, 189–208. doi:10.1007/BF00158428.
- Utz, D., Hanslmeier, A., Muller, R., Veronig, A., Rybák, J., Muthsam, H.: 2010, Dynamics of isolated magnetic bright points derived from Hinode/SOT G-band observations. *Astron. Astrophys.* **511**, A39. doi:10.1051/0004-6361/200913085.
- Vorpahl, J., Pope, T.: 1972, Solar Bright Points in 3840 Å and H α . *Solar Phys.* **25**, 347–356. doi:10.1007/BF00192334.
- Watanabe, H., Vissers, G., Kitai, R., Rouppe van der Voort, L., Rutten, R.J.: 2011, Ellerman Bombs at High Resolution. I. Morphological Evidence for Photospheric Reconnection. *Astrophys. J.* **736**, 71. doi:10.1088/0004-637X/736/1/71.
- Wöger, F., von der Lühe, O., Reardon, K.: 2008, Speckle interferometry with adaptive optics corrected solar data. *Astron. Astrophys.* **488**, 375–381. doi:10.1051/0004-6361:200809894.
- Zachariadis, T.G., Alissandrakis, C.E., Banos, G.: 1987, Observations of Ellerman bombs in H-alpha. *Solar Phys.* **108**, 227–236. doi:10.1007/BF00214163.

